Acta Cryst. (1985). B41, 33-41

The Structure of the *A*-Cation-Deficient Perovskite UNb_4O_{12}

BY M. LABEAU

Institut National Polytechnique de Grenoble, Laboratoire de Génie Physique, BP 46, 38402 *St Martin D'Hères, France*

AND I. E. GREY,* J. C. JOUBERT, J. CHENEVAS, A. COLLOMB AND J. C. GUITEL

Laboratoire de Cristallographie, CNRS, 166*X*, 38042 *Grenoble, France*

(*Received* 12 *March* 1984; *accepted* 3 *September* 1984)

Abstract

The compound UNb_4O_{12}, when prepared by slow cooling in vacuum from 1573 K, displays a pseudotetragonal perovskite superstructure with $a \simeq 4a_p = 15{\cdot}424\,(2)$, $c \simeq 4a_p = 15{\cdot}592\,(1)$ Å. Electron-microscopy studies show it has a microdomain structure in the *ab* plane and the apparent tetragonal symmetry is due to interchange of *a* and *b* of an orthorhombic structure in domains of size ~200 Å. The structure was determined by a method of successive approximations, using different groupings of the superlattice reflections that could be indexed by subcells of the $4\times4\times4$ superlattice and could be associated with particular structural features. A close approximation to the average structure in a single domain was obtained in a $4\times2\times4$ supercell, space group *Immm*. It comprises a face-centred array of [010] columns of U atoms in alternate (001) planes. The column ordering along [100] is not fully developed and can be described by a sinusoidal modulation. The framework of NbO_6 octahedra distorts to reduce the coordination number and U–O bond lengths of the U atoms from the cuboctahedral coordination of ideal perovskite. The anion displacements may be resolved into an octahedral tilt component about [101] axes plus a displacement component due to the U/vacancy distribution. The octahedral tilt system may be described as twinned $a^-b^0c^-$ of magnitude ~6°. Regular twinning of the tilted octahedra on (100) and (001) planes gives rise to a characteristic splitting of the tilt reflections.

1. Introduction

The reactions of uranium and thorium dioxides with niobium pentoxide were first studied by Kovba & Trunov (1962). Both dioxides form the same type of compound, $MO_2.(Nb_2O_5)_2$, with structures closely related to that of perovskite. Kovba & Trunov observed a number of superstructure lines in the powder X-ray diffraction pattern which they indexed with a tetragonal cell, $a = a_p \simeq 3{\cdot}9$, $c = 2a_p \simeq 7{\cdot}8$ Å.† In a later study, Trunov & Kovba (1966) reported the structure determination for the thorium compound, $ThNb_4O_{12}$. They showed that the doubling of the a_p axis was due to ordering of Th atoms and vacancies in the cuboctahedral sites in alternate $(001)_p$ layers, *i.e.* layers of cuboctahedra statistically half-filled by Th atoms alternate with empty layers along **c**.

We have recently reported the results of single-crystal X-ray and electron diffraction/microscopy studies on $ThNb_4O_{12}$ in which weak, superlattice reflections, in the form of diffuse streaks, were observed and interpreted to be due to short-range ordering of Th atoms and vacancies in the half-filled (001) layers (Alario-Franco, Grey, Joubert, Vincent & Labeau, 1982; Labeau, Grey, Joubert, Vincent & Alario-Franco, 1982). The type of ordering was found to depend on the cooling rate of the samples. In quenched samples the Th atoms and vacancies are ordered in alternate chains parallel to $[100]_p$ or $[010]_p$ whereas in the slow-cooled samples, ordering of columns along $[110]_p$ or $[\bar{1}10]_p$ occurs. In both cases the ordering occurs in microdomains and the correlation length along the chains/columns is only ~ 20–50 Å. Other diffuse reflections were shown to be due to tilting of the octahedral framework. These reflections, centred at $(h/2, k/2, l/2)_p$, were split into clusters of four satellites due to periodic twinning of the tilt system at the microdomain boundaries.

We have extended our structural studies to the uranium niobate UNb_4O_{12}, and have observed weak superlattice reflections which could not be indexed on the tetragonal cell reported for UNb_4O_{12} by Kovba & Trunov (1962). The diffraction patterns observed for both quenched and slow-cooled samples differ from those for $ThNb_4O_{12}$, indicating that both the metal-vacancy ordering in the (001) planes and the octahedral tilt system are different for UNb_4O_{12}. We collected an X-ray intensity data set from a macroscopic single crystal of slow-cooled UNb_4O_{12} and

* Permanent address: CSIRO Division of Mineral Chemistry, PO Box 124, Port Melbourne, Victoria 3207, Australia.

†Throughout this paper, subscript *p* refers to the simple cubic perovskite aristotype. If not subscripted, indices and directions refer to the superstructure under discussion.

0108-7681/85/010033-09$01.50

carried out a structure determination and refinement, the results of which are reported here, together with preliminary observations on the quenched sample.

2. Experimental

2.1. *Preparation and characterization*

UNb_4O_{12} was prepared from a mixture of analytical grade Nb_2O_5, NbO_2 (Johnson Matthey) and U_3O_8 (Merck) according to the molar proportions $U_3O_8 + 4NbO_2 + 4Nb_2O_5$. The weighed mixture was finely ground, pelleted and sealed under vacuum in a silica tube. The sample was heated for 3 d at 1573 K and then cooled to 473 K at a cooling rate of 15 K h^{-1}. A second sample was heated for 3 d at 1573 K then quenched in ice water.

Accurate lattice parameters for the slow-cooled phase were determined by refinement of the 2θ values obtained with a Guinier focusing camera, using Fe $K\alpha$ radiation, and with silicon as an internal standard. The refined values for the tetragonal cell are $a = 3{\cdot}856\,(1)$, $c = 7{\cdot}796\,(1)$ Å, $c/a = 2{\cdot}022$.

Electron diffraction/microscopy studies were carrried out with a Jeol 200CX electron microscope. Samples for study were crushed in an agate mortar and suspended in *n*-butanol, then transferred to holey-carbon-coated copper grids.

2.2. *Single-crystal X-ray diffraction and data collection*

Single-crystal diffraction patterns were obtained by the precession method. Exposure times of up to 100 h were needed to record the weak superlattice reflections, particularly those associated with tilting of the octahedra.

For the intensity-data collection on slow-cooled UNb_4O_{12}, a macroscopically untwinned crystal in the form of a cube, with edge 0·12 mm, was used. Intensities were collected on a Philips PW 1100 diffractometer with Mo $K\alpha$ radiation monochromated by a flat graphite crystal. Operating features: angular range, $2{\cdot}5 \le \theta \le 26°$; scan mode, θ–2θ; scan range, $S = (1{\cdot}60 + 0{\cdot}30 \tan\theta)°$; scan speed, $0{\cdot}04° s^{-1}$.

To improve the counting statistics for the weak superlattice reflections, scanning mode SMO2 was used, involving multiple scans (maximum four) to attain a preset number of counts (6000). A full sphere of data, without restrictions, was collected in the range $2{\cdot}5 \le \theta \le 16{\cdot}5°$. For θ between 16·5 and 26°, an *I*-centring restriction was imposed, because reflections violating the *I*-centring condition were very weak and restricted to low angles. A total of 4126 reflections were collected and reduced to structure amplitudes by applying Lorentz, polarization and spherical absoprtion corrections ($\mu = 216$ cm^{-1}). An examination of equivalent high-angle reflections showed no significant deviation from the tetragonal symmetry, and averaging of equivalent reflections according to Laue symmetry $4/mmm$ gave 952 independent reflections. Of these, 288 were extremely weak and only one equivalent was accepted for measurement in the data collection. These were not used in the refinement. The remaining 644 reflections had an average internal agreement factor $[\sum(|F^2_{eq} - \bar{F}^2|)/\sum F^2_{eq}]$ for equivalent reflections of 0·06, and 528 had significant intensity with $F^2 > 2\sigma(F^2)$.

Refinement was carried out using the *XRAY*76 series of programs (Stewart, 1976), and *POWDER* (Rossell & Scott, 1975), a full-matrix least-squares program based on *ORFLS* (Busing, Martin & Levy, 1962). The refinements with *POWDER* were based on F^2; the quantity minimized is $\sum w(F_o^2 - F_c^2)^2$, where $w = 1/(F_o^2 + F^2_{min})$. The residual used is $R = \frac{1}{2}[\sum w(F_o^2 - F_c^2)^2/\sum wF_o^4]^{1/2}$ and is numerically comparable to the weighted residual commonly quoted for single-crystal structure refinements (Rossell & Scott, 1975).

Scattering factors for neutral atoms, with corrections for anomalous dispersion, were taken from *International Tables for X-ray Crystallography* (1974).

3. Electron diffraction/microscopy studies

The complete reciprocal lattices of both quenched and slow-cooled samples of UNb_4O_{12} were established from electron diffraction studies. The diffraction patterns for both phases displayed strong, sharp reflections that could be indexed by a tetragonal cell with $a = a_p \simeq 3{\cdot}85$, $c = 2a_p \simeq 7{\cdot}79$ Å, consistent with the observations of Kovba & Trunov (1962). Further weak superlattice reflections and diffuse streaks that could not be indexed on the above cell were observed. The extra diffraction effects were quite different for the quenched and slow-cooled samples; the observations are summarized in Fig. 1, where the reciprocal lattices for both samples are compared with those for slow-cooled $ThNb_4O_{12}$ (Alario-Franco *et al.*, 1982) and for $Na_{0{\cdot}7}Th_{0{\cdot}075}NbO_3$ (Labeau, 1980).

3.1. *Quenched* UNb_4O_{12}

The reciprocal lattice for the quenched phase is shown in Fig. 1(*a*). The groupings of four diffuse rods in the form of squares, with sides parallel to $g(110)_p$ and $g(\bar{1}10)_p$, are the same as observed for slow-cooled $ThNb_4O_{12}$, Fig. 1(*c*), and so by analogy are due to ordering of $[110]_p$ and $[\bar{1}10]_p$ columns of U atoms in alternate $(001)_p$ layers. The ordering occurs in microdomains and the length of the rods corresponds to correlation lengths of only 20–30 Å in individual domains of UNb_4O_{12}.

Also shown in Fig. 1(*a*) are four diffuse streaks, extending from the body centre of the perovskite reciprocal-lattice subcell to each of the four equatorial face centres in the a^*b^* plane, *i.e.* diffuse streaks are parallel to $g(100)_p$ and $g(010)_p$. Along the third direction, $g(001)_p$, pairs of discrete reflections occur, at

$(h/2, k/2, l/2\pm\frac{1}{4})_p$, which are slightly elongated along $g(001)_p$. A similar grouping of diffuse streaks occurs in $Na_{0.7}Th_{0.075}NbO_3$ (Labeau, 1980), although, as seen in Fig. 1(*d*) for this compound, pairs of streaks occur along all three cubic reciprocal perovskite directions, $g\{100\}_p$. This type of observation has been interpreted by Dénoyer, Comès, Lambert & Guinier (1974) (for the case of cubic $NaNbO_3$) as due to planar disorder of octahedral tilting about the three cubic perovskite axes.

By analogy, the diffuse streaks parallel to $g(100)_p$ and $g(010)_p$ can be interpreted as due to uncorrelated rotations of the octahedra about a_p and b_p rotation axes in successive $(100)_p$ and $(010)_p$ layers respectively, together with correlated rotations about c_p such that the sense of the rotation alternates in successive $(001)_p$ planes, giving an $a^{\pm}a^{\pm}c^-$ tilt system, using Glazer's (1972) terminology. The pairs of satellites along $g(001)_p$ may be interpreted as resulting from periodic twinning of the tilt system across (001), *cf.* $ThNb_4O_{12}$ (Labeau *et al.*, 1982). The separation between the satellites is $2M^*$ where M is the twin-plane separation. The observed separation corresponds to a twinning on alternate $(001)_p$ planes. The twin-plane spacing thus corresponds to the periodicity of occupied and vacant $(001)_p$ layers of U atoms.

3.2. *Slow-cooled* UNb_4O_{12}

In contrast to the diffraction patterns for $ThNb_4O_{12}$ and quenched UNb_4O_{12}, those for slow-cooled UNb_4O_{12}, Fig. 1(*b*), showed no diffuse diffraction effects; all the superlattice reflections were discrete and quite sharp, and could be indexed with a tetragonal superlattice with $a \simeq 4a_p = 15{\cdot}42$, $c \simeq 4a_p = 15{\cdot}59$ Å. By analogy with the patterns for the other compounds, the superlattice reflections could be divided into two main sets, having U/vacancy ordering (large filled circles) and octahedral tilts (small filled circles) respectively, as their dominant structural origins. The two sets of reflections had quite different intensity ranges and θ dependencies. The intensities of the U/vacancy ordering reflections were stronger, by a factor of about 10, than the tilt reflections, and showed no noticeable dependence on diffraction angle, whereas the intensities of the tilt reflections decreased rapidly with increasing θ.

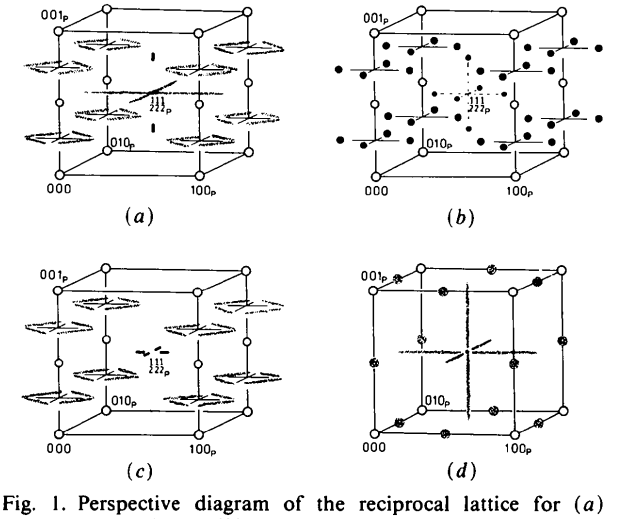

Fig. 1. Perspective diagram of the reciprocal lattice for (*a*) quenched UNb_4O_{12}, (*b*) slow-cooled UNb_4O_{12}, (*c*) slow-cooled $ThNb_4O_{12}$ and (*d*) $Na_{0.7}Th_{0.075}NbO_3$.

3.2.1. U/*vacancy ordering reflections.* These reflections occur in clusters of four, made up of two intersecting pairs oriented parallel to a^* and b^* respectively. Dark-field images obtained for the two pairs of satellites showed that they derived from different small regions of the crystal, with average size ~200 Å. Thus slow-cooled UNb_4O_{12} has a microdomain texture, in which the U/vacancy ordering occurs in planes parallel to $(100)_p$ and $(010)_p$ respectively in the two domain orientations. The observed tetragonal symmetry is thus representative of the average structure, and lower-symmetry local structures can occur in the microdomains.

3.2.2. *Tilt reflections.* When UNb_4O_{12} is cooled slowly, the diffuse streaks observed in the quenched samples, parallel to $g(100)_p$ and $g(010)_p$, disappear and are replaced by discrete spots: around each node $(h/2, k/2, l/2)_p$, h, k, l odd, there is an octahedron of satellites at $(h/2\pm\frac{1}{4}, k/2, l/2)_p$, $(h/2, k/2\pm\frac{1}{4}, l/2)_p$ and $(h/2, k/2, l/2\pm\frac{1}{4})_p$. For those nodes with two indices equal, only four of the six satellites were observed, *e.g.* for $h = k$ the pair of satellites along $g(001)_p$ was missing. By analogy with the results previously obtained for $ThNb_4O_{12}$ (Labeau *et al.*, 1982), these results may be interpreted in terms of a microdomain model. The observed satellite groupings may be considered to result from the superposition of two sets of satellites, arising from an $a^-b^0c^-$ tilt system in one microdomain orientation and an $a^0b^-c^-$ tilt system in the other orientation. In both microdomains, periodic twinning of the tilt system occurs across alternate $(001)_p$ and $(100)_p$ planes.

Dark-field electron-microscope images were obtained using superlattice reflections split parallel to a^* and b^* respectively. The images showed that the reflections originated from diffraction in different regions of the crystal and that the tilt system was correlated with the U/vacancy ordering in the individual microdomains.

4. Structure determination and refinement

The microdomain character of the crystals of UNb_4O_{12} makes a structure determination and refinement by normal procedures impracticable.

Instead, we have approached the structure analysis by a method of successive approximations whereby

Table 1. *Classification of superlattice reflections for* UNb_4O_{12}

Reflection type	Microdomain	Reflection indices ($4\times4\times4$ supercell)	Intensity range	Unit cell	Comments
1	1+2	$4n, 4n, 4n+2$	100-5000	$a_p\times a_p\times 2a_p$ $P4/mmm$	Ordering of U atoms in alternate $(001)_p$ planes
2(*a*)	1	$2n+1, 4n, 2n+1$	10-700	$4a_p\times a_p\times 4a_p$ *B*-centred orthorhombic cell	Ordering of $[010]_p$ columns of U atoms *within* occupied $(001)_p$ layers
2(*b*)	2	$4n, 2n+1, 2n+1$			
3(*a*)	1	$2n+1, 4n+2, 4n+2$	6-60	$4a_p\times 2a_p\times 4a_p$ *I*-centred cell	Periodic twinning of octahedral tilt system. Reflection intensities diminish rapidly with *increasing* θ for 3(*a*), (*b*), less rapidly for 3(*c*) reflections
3(*b*)	2	$4n+2, 2n+1, 4n+2$			
3(*c*)	1+2	$4n+2, 4n+2, 2n+1$			
4(*a*)	1	$4n, 4n+2, 2n+1$	6-35	$2a_p\times 2a_p\times 4a_p$ *P* cell (when grouped with 3*c* reflections)	Ordering of U atoms along $[010]_p$ columns
4(*b*)	2	$4n+2, 4n, 2n+1$			
5	1+2	$2n+1, 2n+1, 2n$	6-60	$4a_p\times 4a_p\times 2a_p$ *C*-centred cell	$\langle 110\rangle_p$ modulation of U atom/vacancy ordering

the intensity data set is divided into different groupings of reflections such that each grouping can be indexed by a subcell of the complete $4a_p\times4a_p\times4a_p$ superlattice and can be associated with a particular structural feature. Each of the data sets is analysed in turn, starting with the strongest group of reflections and going to progressively weaker sets.

On the basis of intensity ranges, dependence on diffraction angle and extinction rules, five groupings of superlattice reflections were identified for slow-cooled UNb_4O_{12}. They are listed in Table 1 and their analyses will be considered in turn below.

4.1. *Type* 1 *reflections*

These are the strongest group of superlattice reflections, corresponding to a doubling of one of the perovskite subcell parameters, to give a $1\times1\times2$ tetragonal superstructure. By analogy with other *A*-cation-deficient perovskites such as $LaNb_3O_9$ (Iyer & Smith, 1967) and $ThNb_4O_{12}$ (Trunov & Kovba, 1966), this axial doubling was interpreted as due to ordering of U atoms in alternate $(001)_p$ layers of cuboctahedra. The structural parameters for $ThNb_4O_{12}$ in space group $P4/mmm$ (Trunov & Kovba, 1966) were used as starting parameters for a refinement using 98 subcell and type 1 reflections. Refinement of positional and isotropic thermal parameters converged at $R=0{\cdot}063$. The final parameters are given in Table 2.*

The refinement confirmed that the U atoms are ordered into every second $(001)_p$ layer of cuboctahedral sites, but the unit cell does not allow any ordering *within* these layers. The condensation of the real structure in the $1\times1\times2$ cell results in a statistical half-occupany of all cuboctahedral sites in the occupied (001) layers. The very large thermal parameters for the O atoms, Table 2, indicate that the anions have large displacements from the positions allowed in the space group $P4/mmm$.

A difference Fourier map in which the F_c's were phased by the (001) U ordering (all atoms in ideal pervoskite positions) gave useful information on the directions and approximate magnitude of the major atomic displacements that could be used as constraints in further developments of the structural model. An analysis showed:

(*a*) The major Nb displacements are along [001], *away* from the layers of U atoms.

(*b*) The apical O sites O(1) and O(2) are both surrounded by rings of residual intensity in the *ab* plane, with a radius of about 0·5 Å. For O(2), which lies in the (001) occupied layer of U atoms, the ring is displaced slightly along [001], and there is a modulation of the intensity around the ring, with weak maxima along $\langle110\rangle$. For O(1), the modulation is much more pronounced and well defined maxima occur along $\langle110\rangle$.

(*c*) The equatorial oxygen O(3) has a major peak that is elongated between $\sim\langle102\rangle$ and $\langle201\rangle$, with the *c* component *towards* the occupied U layer.

(*d*) No displacement of the U atoms could be discerned from the ΔF map.

4.2. *Type* 2 *reflections*

These reflections form a well defined grouping, for which the intensities are an order of magnitude smaller than those of the type 1 reflections, but are an order of magnitude greater than those of other groupings. They are represented by large filled circles in Fig. 1(*b*) and are primarily due to U/vacancy ordering in the occupied (001) layers. The reflections may be divided into two sets, representing ordering in the two microdomain orientations. There is no overlap of reflections from the two sets and so one set can be selected and analysed to determine the U/vacancy order corresponding to a single domain orientation. Thus, in the following analysis we will consider only reflections of the type 2(*a*), Table 1, which can be indexed in a $4\times1\times4$ *B*-centred orthorhombic cell.

* Lists of structure factors have been deposited with the British Library Lending Division as Supplementary Publication No. SUP39714 (13 pp.). Copies may be obtained through The Executive Secretary, International Union of Crystallography, 5 Abbey Square, Chester CH1 2HU, England.

Table 2. *Parameters from refinement of type* 1 *reflections*

Unit cell: tetragonal, $P4/mmm$, $a = b = 3{\cdot}856\ (1)$, $c = 7{\cdot}796\ (1)$ Å

	x	y	z	B(Å^2)
U	0	0	0	0·72 (9)
Nb	$\frac{1}{2}$	$\frac{1}{2}$	0·2611 (6)	1·32 (7)
O(1)	$\frac{1}{2}$	$\frac{1}{2}$	0	5·8 (1·8)
O(2)	$\frac{1}{2}$	0	$\frac{1}{2}$	5·9 (1·6)
O(3)	0	$\frac{1}{2}$	0·2285 (31)	5·3 (0·7)

In the centrosymmetric space group *Bmmm*, two alternative models are possible, with the unit-cell origin located at a U-atom site, model 1, or between a pair of U atoms, model 2. These are illustrated in Fig. 2. Model 2 is fully ordered, with pairs of occupied [010] rows of U atoms alternating with two empty rows, whereas model 1 is partially ordered, with successive [010] rows being fully occupied, statistically half occupied and empty. Guided by the results from the analysis of the type 1 reflections and by our previous studies on $ThNb_4O_{12}$ (Alario-Franco *et al.*, 1982), approximate magnitudes and directions of the U- and Nb-atom displacements were estimated for both models and used as starting parameters in refinements with all 225 type 2 reflections. With metal atoms only, model 1 refined to an R value of 0·13 whereas model 2 would not refine below $R = 0{\cdot}22$.

In a second series of refinements, disorder between the filled and empty sites was allowed in both models. With refinement of the population parameters of the U atoms, both models refined to the *same* R value of 0·12, with site occupancies along [100] of 0·5, 0·9, 0·5, 0·1, 0·5 ... and 0·8, 0·8, 0·2, 0·2, 0·8 ... for models 1 and 2. The two distributions represent the same sinusoidal modulation with a change of phase only.

High-resolution electron-microscope (HREM) images were taken along [010] and the projected charge density in the *ac* plane, shown in Fig. 3, is generally consistent with model 1, *i.e.* intensities of white spots corresponding to vacant cuboctahedral sites along [100] in the underfocused image vary in the sequence strong, weak, absent, weak, strong ... rather than in the sequence medium, medium, weak, weak ... required for model 2. This latter sequence was occasionally observed but it appeared to be due to overlap of two regions of model 1 structure in projection. Detailed discussion of the HREM studies will be subsequently reported. For the structure determination, model 1 was adopted.

A difference Fourier map was calculated at this stage and it showed the positions of all O atoms. The major displacements correlated clearly with the U/vacancy ordering; those O atoms closest to the 'fully' occupied (p.p. = 0·9) rows of U atoms were displaced by ~0·4 Å *towards* the U atoms.

In addition to those anion displacements related to the U ordering, the ΔF map also showed pairs of peaks along $[\bar{1}01]$ and $[10\bar{1}]$, symmetrically distributed about the positions of the anions in the *ac* plane at $y = 0$. These peaks were consistent with a model involving cooperative tilting of octahedra about [101], *i.e.* tilt system $a^-b^0c^-$. Such a model requires a doubling of the *b* axis, to be described in § 4.3.

4.3. *Type* 3 *and* 4 *reflections*

As discussed in § 3.2.2, the type 3 reflections, represented by small filled circles in Fig. 1(*b*), have their origin in a regular tilting of the octahedral framework, which is periodically twinned at $\{100\}_p$ planes. Electron-microscopy studies showed that the tilt system was correlated with the U/vacancy ordering in the two microdomain orientations. For the microdomains containing $[010]_p$ columns of U atoms, discussed in

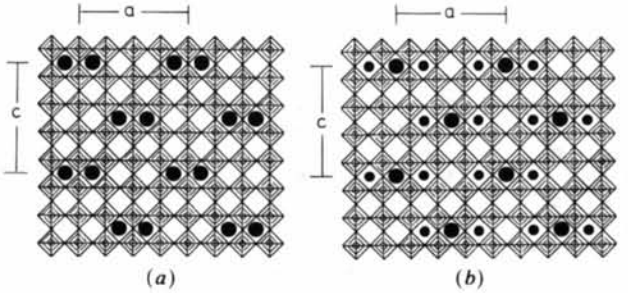

Fig. 2. Alternative models for U/vacancy ordering in the occupied (001) layers of UNb_4O_{12}, viewed along **b** in the $4 \times 1 \times 4$ supercell, *Bmmm*. Large and small filled circles represent filled and half-filled U sites.

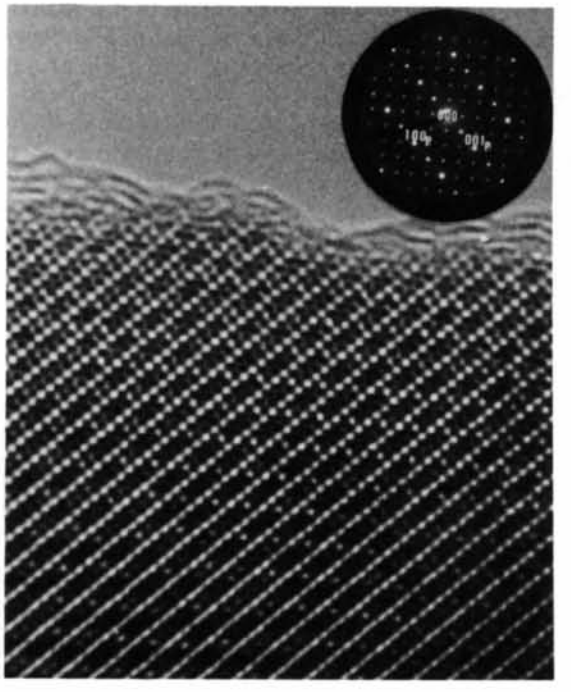

Fig. 3. HREM image of slow-cooled UNb_4O_{12}, along [010]. The white dots correspond to empty cuboctahedral sites.

§ 4.2, the tilt system is $a^-b^0c^-$, which gives rise to the reflections 3(*a*) and 3(*c*) in Table 1. These may be indexed in an *I*-centred $4\times2\times4$ orthorhombic supercell. The doubling of the *b* axis allows the possibility of a modulation of the U-atom occupancy of those sites which were established to be half filled in the analysis given in § 4.2. Such a modulation, due to local ordering of alternately filled and empty sites along **b**, would give rise to reflections of the type (2*n*, 2*n*+1, 2*n*+1) in the $4\times2\times4$ supercell, *i.e.* types 3(*c*) and 4(*a*) reflections. The systematic extinctions for the types 1-4 reflections in the $4\times2\times4$ cell include, in addition to those required by the body centring, the condition *hk*0, $h=2n+1$. This gives the space group as *Imma*. However, it was not possible to modulate the U occupancy of the half-filled sites in this space group. It was thus assumed that $h=2n+1$ for *hk*0 was a structural extinction and the space group was reduced to *Immm*. The U modulation was estimated by hand calculation of structure factors for low-angle type 4(*a*) reflections (where contributions due to metal-atom displacements are smallest).

Using the atomic coordinates obtained from the analysis of the type 2 reflections as a guide, the O displacements consistent with a twinned $a^-b^0c^-$ tilt system were estimated and used as starting parameters for a refinement. Starting parameters for the metal atoms also came from the refinement in the $4\times1\times4$ cell. The refinement was initially carried out with types 2(*a*), 3(*a*) and 4(*a*) reflections which derive from a common microdomain orientation, and Fourier maps were used to check the atom coordinates. When all atoms were considered to be correctly located, the refinement was extended to all observed subcell and types 1-4 reflections, using the program *POWDER* (Rossell & Scott, 1975) that allowed the F^2 contributions for equivalent reflections in the two microdomain orientations to be summed, *i.e.* it was assumed that there was no correlation between the ordering in the two types of microdomain. Refinement of all coordinates and group isotropic thermal parameters for U, Nb and O converged at $R=0{\cdot}053$ for the 376 subcell and types 1-4 reflections. The final parameters are listed in Table 3.*

* See deposition footnote.

Table 3. *Refined model for* UNb_4O_{12} *from analysis of types* 1-4 *reflections*

Unit cell: orthorhomic, *Immm*, $a=15{\cdot}424\,(2)$, $b=7{\cdot}712\,(1)$, $c=15{\cdot}592\,(1)$ Å; $B(U)=0{\cdot}45\,(2)$, $B(Nb)=0{\cdot}67\,(3)$, $B(O)=1{\cdot}20\,(22)$ Å^2

	Site occupancy	*x*	*y*	*z*
U(1)	0·88 (2)	0	0	0
U(2)	0·96 (2)	0	½	0
U(3)	0·55 (2)	0·2591 (8)	0	0
U(4)	0·46 (3)	0·2576 (13)	½	0
U(5)	0·06 (1)	0·490 (2)	0	0
U(6)	0·06 (1)	0·486 (2)	½	0
Nb(1)		0·1257 (4)	0·2521 (13)	0·1352 (1)
Nb(2)		0·3803 (3)	0·2640 (7)	0·1251 (2)
O(1)		0·384 (4)	0	0·098 (4)
O(2)		0·149 (4)	0	0·364 (3)
O(3)		0·093 (4)	0	0·136 (3)
O(4)		0·369 (5)	0	0·404 (3)
O(5)		0·362 (3)	0·285 (5)	0
O(6)		0	0·227 (7)	0·391 (3)
O(7)		0·135 (3)	0·185 (6)	0
O(8)		0	0·278 (7)	0·100 (3)
O(9)		0·247 (2)	0·214 (6)	0·131 (3)
O(10)		0·137 (4)	0·291 (5)	0·253 (1)

4.4. *Type* 5 *reflections*

These are a very weak subset of superlattice reflections which were observed to be somewhat more diffuse than the other reflections. The reflections were confined to half-integral layers along **c*** of the reciprocal perovskite subcell and could all be indexed with a *C*-centred $4\times4\times2$ orthorhombic supercell.

The distribution of reflection intensities displayed an unusual set of structural extinctions which assisted in the determination of a structural model for the U modulation and associated displacements. The observed intensity distributions in (*hk*0), (*hk*1) and (*hk*2) layers are shown in Fig. 4. Only first-order satellites were observed, indicating that the structural effects giving rise to the type 5 reflections could be modelled by a sinusoidal modulation. The uniform intensity distribution and small θ dependence of the reflections with $l=2n+1$ suggested that their origin was due predominantly to a modulation of the U-atom site occupancies. From structure factor calculations for low-angle (*hk*1) reflections, the approximate amplitude of the sinusoidal modulation of site occupancies along the [010] rows was established,

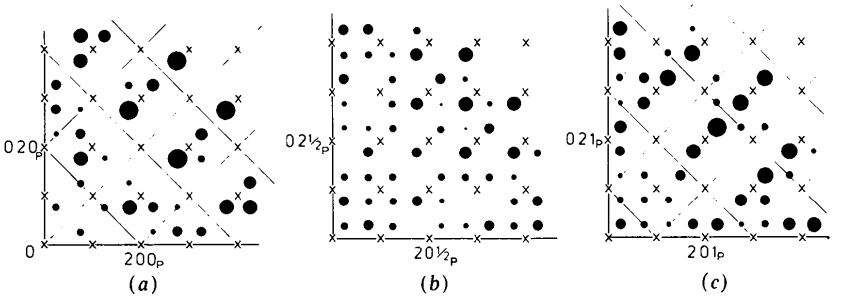

Fig. 4. Schematic representation of observed distribution of type 5 reflections in (*a*) $(hk0)_p$, (*b*) $(hk\frac{1}{2})_p$ and (*c*) $(hk1)_p$. The area of the circles is proportional to F_o^2. Subcell reflections are marked with crosses.

Table 4. *Parameters from refinement of type 5 reflections*

Unit cell: orthorhombic, *Immm*, $a = 15{\cdot}424\ (2)$, $b = 15{\cdot}424\ (2)$, $c = 15{\cdot}592$ Å; $B(\mathrm{U}) = 0{\cdot}5$ Å^2, $B(\mathrm{Nb}) = 0{\cdot}5$ Å^2

	Site occupancy	x	y	z
U(1)	1·0	0	0	0
U(2)	0·9	0	0·250	0
U(3)	0·8	0	$\frac{1}{2}$	0
U(4)	0·4	0·255 (1)	0	0
U(5)	0·4	0·2558 (5)	0·272 (3)	0
U(6)	0·6	0·250	$\frac{1}{2}$	0
U(7)	0·1	$\frac{1}{2}$	0·250	0
U(8)	0·2	$\frac{1}{2}$	$\frac{1}{2}$	0
Nb(1)		0·124 (2)	0·131 (2)	0·125
Nb(2)		0·385 (2)	0·130 (2)	0·125
Nb(3)		0·384 (2)	0·368 (2)	0·125
Nb(4)		0·125	0·375	0·125

and then U-atom displacements were calculated to give the observed intensity distribution as a function of θ. Directions and approximate magnitudes of the Nb displacements were estimated by structure factor calculations for the ($hk0$) and ($hk2$) reflections and used as starting parameters for a refinement based on F^2, in which the contributions from the two microdomain orientations were assumed to be equal and uncorrelated, and were summed as $F^2(hkl) + F^2(khl)$. The model was constructed in the full $4\times4\times4$ cell, space group *Immm*, to allow integration with the previous models. For the model including metal atoms only, refinement of atomic coordinates and U population parameters converged at an R value of 0·22, for the 115 type 5 reflections. It was not possible to locate the O atoms by Fourier methods because the intensity of each reflection was contributed to by both microdomain orientations. The refined parameters are given in Table 4.*

4.5. *The complete model*

The complete data set can be indexed in a primitive $4\times4\times4$ supercell. A model was constructed for the complete structure in one microdomain orientation, by combining, in the $4\times4\times4$ cell, space group *Pmmm*, the structural data obtained from the individual analyses. A refinement of the metal-atom coordinates was carried out using the *POWDER* refinement program. The refinement converged at $R = 0{\cdot}057$ for all 528 reflections with $F^2 > 2\sigma(F^2)$. However, attempts to refine the O coordinates were not successful. The coordinate displacements oscillated due to correlations between anions related by the $4\times2\times4$ I-centred cell.

In view of the lack of success in refining the O positions in the $4\times4\times4$ supercell, we confine further discussion, and description of the structure, to the model established in the I-centred $4\times2\times4$ supercell.

* See deposition footnote.

Table 5. *Bond lengths* (Å) *for* UNb_4O_{12}

U(1)-4 O(7)	2·53 (5)	U(2)-4 O(8)	2·31 (5)
-4 O(3)	2·56 (5)	-4 O(4)	2·51 (7)
-4 O(8)	2·65 (5)	-4 O(7)	3·20 (5)
U(3)-2 O(7)	2·38 (5)	U(4)-2 O(5)	2·30 (4)
-O(1)	2·46 (6)	-2 O(4)	2·46 (7)
-2 O(9)	2·63 (5)	-2 O(2)	2·57 (5)
-2 O(5)	2·71 (4)	-2 O(9)	3·01 (5)
-2 O(3)	3·33 (6)	-2 O(7)	3·07 (5)
U(5)-2 O(1)	2·25 (7)	U(6)-4 O(6)	2·46 (5)
-2 O(1)	2·48 (7)	-2 O(5)	2·54 (5)
-4 O(6)	2·71 (5)	-2 O(5)	2·88 (5)
-2 O(5)	2·96 (5)	-2 O(2)	2·97 (6)
-2 O(5)	3·18 (5)	-2 O(2)	3·29 (6)
Nb(1)-O(10)	1·86 (2)	Nb(2)-O(6)	1·86 (1)
-O(9)	1·89 (3)	-O(2)	1·88 (2)
-O(3)	2·01 (2)	-O(10)	1·97 (2)
-O(4)	2·01 (2)	-O(5)	1·98 (1)
-O(8)	2·02 (1)	-O(1)	2·08 (1)
-O(7)	2·17 (1)	-O(9)	2·10 (3)
O(9)-O(10)	2·55 (6)	O(8)-O(10)	2·61 (6)
O(3)-O(7)	2·64 (5)	O(2)-O(5)	2·70 (4)
O(3)-O(8)	2·64 (6)	O(1)-O(5)	2·70 (5)
O(4)-O(8)	2·65 (7)	O(1)-O(9)	2·73 (6)
O(7)-O(9)	2·68 (5)	O(2)-O(9)	2·73 (5)
O(7)-O(8)	2·70 (5)	O(5)-O(6)	2·74 (5)
O(4)-O(7)	2·85 (5)	O(5)-O(9)	2·76 (5)
O(3)-O(9)	2·89 (6)	O(1)-O(6)	2·77 (6)
O(4)-O(9)	2·89 (6)	O(2)-O(10)	2·84 (4)
O(4)-O(10)	2·93 (5)	O(1)-O(10)	2·84 (6)
O(3)-O(10)	2·97 (5)	O(2)-O(6)	2·92 (6)
O(8)-O(10)	3·18 (5)	O(6)-O(10)	3·06 (6)

As discussed in § 4.3, this model accounts satisfactorily for all the types 1–4 superlattice reflections and incorporates both the U/vacancy ordering (and associated atomic displacements) and the tilting and distortion of the octahedral framework. Because of the microdomain character of the crystal studied, both these structural effects are, of course, averaged over both intradomain and interdomain variations.

5. Description of the structure

From the atomic coordinates given in Table 3, bond lengths for the U- and Nb-centred polyhedra were calculated and are given in Table 5. A projection of the structure on (010) is shown in Fig. 5 and a (001) section through the structure at $z = 0$ is given in Fig. 6. The modulation of the U-atom site occupancies is illustrated by the size of the filled circles. The half-filled rows of U atoms [U(3), U(4)] are displaced away from the filled rows [U(1), U(2)] by $\sim 0{\cdot}17$ Å along $[100]_p$. The U atoms in the minority sites [U(5), U(6), p.p. = 0·1] occupy split positions displaced by about 0·2 Å on either side of the mirror plane at $x = \frac{1}{2}$, indicating that the symmetry for the local-atom ordering is lower than that allowed by *Immm*.

The Nb atoms closest to the filled rows of U atoms are displaced by 0·15 Å along [001] towards the unoccupied layers. The second independent Nb atom is displaced by about the same distance along [110], also towards a region where the U occupation is low.

The largest modifications to the ideal perovskite structure are associated with the framework of NbO_6 octahedra and may be divided into two types: those due to regular tilting of the corner-connected octahedra and those due to local distortions of the octahedra in response to the U/vacancy ordering. The combined effect is a crumpling of the octahedral framework to reduce the bond lengths and coordination number of uranium to oxygen, from the 12-coordinated position it would have in the ideal perovskite structure. For the anions O(1) to O(4), for which the displacements are in the *ac* plane, the observed displacements can each be resolved into a tilt component about [101] plus a displacement component along the tilt axis towards the nearest [010] chain of U atoms. The tilt component for each anion is approximately constant at 6°, and the displacement component is a function of the U occupancy of the nearest [010] chain. For O(1) and O(2), the nearest chain is half occupied [U(3), U(4)] and the displacement component is 0·17 Å whereas for O(3) and O(4) the nearest chain is almost fully occupied [U(1), U(2)] and the displacement component is larger at 0·24 Å. As a result of the combined tilts and distortions of the octahedra, the coordination and bond lengths associated with the different U sites vary considerably. The almost fully occupied site U(1) retains 12 coordination, but with the U–O distances, 2·53–2·65 Å, all shorter than the value of 2·75 Å for ideal perovskite. The second fully occupied site U(2) has approximately cubic coordination, as in UO_2, with two sets of four equal U–O distances at 2·32 and 2·51 Å, and the next-nearest O atoms more than 3 Å away. The coordinations of the two half-occupied sites U(3) and U(4) are also quite different, with ten U(3)–O distances in the range 2·39–2·70 Å, and six U(4)–O distances in the range 2·31–2·57 Å, with all other O atoms more than 3 Å away.

The individual Nb–O bond lengths vary in the range 1·86–2·17 Å, comparable to the ranges observed for $KNbO_3$, 1·86–2·18 Å (Katz & Megaw, 1967) and *P*-$NaNbO_3$, 1·86–2·11 Å (Sakowski-Cowley, Lukaszewicz & Megaw, 1969), which have similar magnitudes of off-centre Nb displacements, 0·17 and 0·13 Å, respectively, *cf.* 0·15 Å for UNb_4O_{12}. However, due to the effect of the U/vacancy ordering, the octahedra are more distorted in UNb_4O_{12} than in the perovskites with all *A*-cation sites occupied by large monovalent cations. For example, in $KNbO_3$ and *N*-$NaNbO_3$ the octahedra are very regular, with O–O distances in the ranges 2·78–2·86 Å and 2·76–2·83 Å, respectively, whereas in UNb_4O_{12} the range of O–O is 2·55–3·18 Å, comparable to the range observed in $PbZrO_3$, 2·52–3·28 Å (Jona, Shirane, Mazzi & Pepinsky, 1957) which has large *A*-cation displacements (0·26 Å). The anion–anion distances generally correlate with the number of near-neighbour U atoms, with the exception of O(10) which has a very long bond to O(8), 3·18 Å, and a short bond to O(9), 2·55 Å. The displacements of the two Nb atoms are towards the two O atoms, O(6) and O(10), that are not coordinated by the major U atoms, giving short Nb(1)–O(10) and Nb(2)–O(6) bonds, 1·86 Å. Electrostatic valence sums were calculated for the metal atoms, using Zachariasen's (1978) parameters, which gave $\sum s = 5{\cdot}0$ for Nb(1) and 5·2 for Nb(2), in good agreement with pentavalent Nb. For U, the calculated valencies were U(1), 3·3; U(2), 3·9; U(3), 3·1; U(4), 3·0; U(5), 3·1 and U(6), 2·7, *i.e.* all less than 4, and in qualitative agreement with the site occupancies being highest for U(1), U(2) and lowest for U(5), U(6).

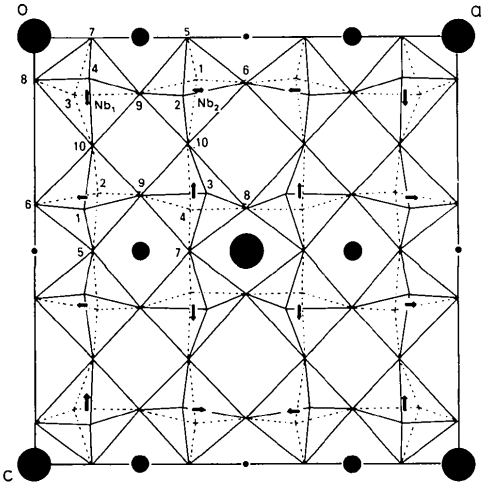

Fig. 5. Projection of the structure of UNb_4O_{12} onto (010) of the 4×2×4 supercell, *Immm*. Nb displacements (exaggerated) shown by arrows. Occupancies of U-atom sites represented by areas of filled circles.

6. Discussion

In common with other *A*-cation-deficient perovskites, such as $LaNb_3O_9$ (Labeau, 1980) and $ThNb_4O_{12}$ (Alario-Franco *et al.*, 1982), UNb_4O_{12} displays a complex hierarchy of ordering patterns of *A* atoms and vacancies in the cuboctahedral sites of the corner-shared octahedral framework. The first stage of the

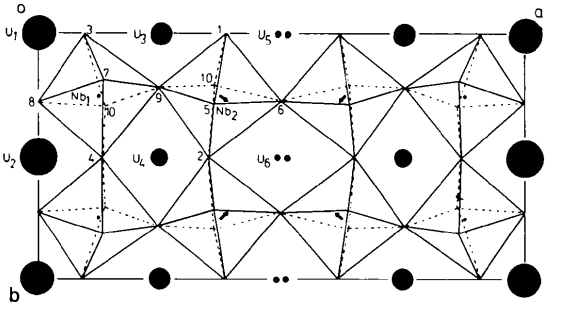

Fig. 6. A (001) section of the structure of UNb_4O_{12}, showing one layer of octahedra centred at $z = \frac{1}{4}$, and a layer of U atoms at $z = 0$.

ordering process involves a migration of A atoms into alternate planes perpendicular to one of the perovskite axes, establishing a tetragonal superlattice with $c = 2a_p$. This primary ordering is evidently established at high temperatures, as even phases quenched rapidly from the melt display superlattice reflections corresponding to the $2a_p$ periodicity (Labeau *et al.*, 1982).

The second stage in the ordering process is the clustering of A atoms within the occupied layers, to form chains, or columns. In $ThNb_4O_{12}$, which was studied in samples quenched directly from the melt, the chains were found to be initially parallel to $[100]_p$ and $[010]_p$, but they quickly rearranged on cooling to form columns of Th atoms along $[110]_p$ and $[\bar{1}10]_p$. In UNb_4O_{12}, we did not study samples quenched from the melt. For samples quenched rapidly from 1573 K, the $\langle 110\rangle_p$ column ordering was already developed. The ordering of columns between successive occupied $(001)_p$ layers is highly correlated, giving a face-centred distribution in the plane perpendicular to the columns, which is coherent over regions of 200–300 Å. Along the columns, the order is short-range in nature, with correlation lengths of only 20–30 Å for both $ThNb_4O_{12}$ and UNb_4O_{12}.

A major difference in ordering between $ThNb_4O_{12}$ and UNb_4O_{12} occurs on slow cooling. Whereas $ThNb_4O_{12}$ retains the $\langle 110\rangle_p$ ordering down to room temperature, the columns of U atoms become reoriented along $[100]_p$ and $[010]_p$ in UNb_4O_{12}. This structural transformation can be explained in terms of nucleation and growth of a microtwin structure at microdomain boundaries in the high-temperature phase. This is illustrated schematically in Fig. 7, where it is evident that twinning of $[110]_p$ and $[\bar{1}10]_p$ columns across $(100)_p$ domain boundaries generates an element of a $[010]_p$ column. Similarly, twinning across $(010)_p$ boundaries leads to nucleation of $[100]_p$ columns. The experimental observations (HREM images) suggest that once nucleated, the two column orientations propagate in different regions of the crystals, forming a new microdomain texture with an average domain size of ~ 200 Å.

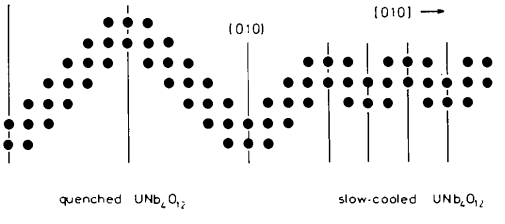

Fig. 7. Schematic representation of the formation of the [010] column structure in UNb_4O_{12} by microtwinning of [110] and $[\bar{1}10]$ columns across (100) boundaries. Filled circles represent U atoms.

The third stage in the hierarchy of ordering of A cations is the development of correlations *along* the columns in the occupied layers. In $ThNb_4O_{12}$ no evidence of ordering of the atoms within the partially occupied $\langle 110\rangle_p$ rows was detected, whereas in UNb_4O_{12} superlattice reflections corresponding to a weak modulation in the *ab* plane were observed. These were of two kinds, listed as type 4 and 5 reflections in Table 1. The former correspond to a partial development of order of alternately filled and empty sites along the statistically half-filled rows whereas the latter may be interpreted as the local development of small regions of a $\langle 110\rangle$ ordering of U atoms in the *ab* plane. Further studies are in progress to elucidate the origins and spatial distributions of the structural effects giving rise to the type 4 and 5 reflections, including HREM studies on samples quenched from different temperatures.

The structure analysis confirms that the observed tetragonal symmetry for UNb_4O_{12} is only apparent and is due to the superposition of two diffraction patterns, each with orthorhombic symmetry, deriving from two microdomain orientations. Such higher pseudosymmetries due to microdomain formation occur commonly in other phases with metal-atom/vacancy ordering, such as sulphide superstructures of the NiAs type (Fleet, 1971; Collin, Chavant & Comès, 1983).

References

ALARIO-FRANCO, M. A., GREY, I. E., JOUBERT, J. C., VINCENT, H. & LABEAU, M. (1982). *Acta Cryst.* **A38**, 177–186.

BUSING, W. R., MARTIN, K. O. & LEVY, H. A. (1962). *ORFLS.* Report ORNL-TM-305. Oak Ridge National Laboratory, Tennessee.

COLLIN, G., CHAVANT, C. & COMÈS, R. (1983). *Acta Cryst.* **B39**, 289–296.

DÉNOYER, F., COMÈS, R., LAMBERT, M. & GUINIER, A. (1974). *Acta Cryst.* **A30**, 423–430.

FLEET, M. E. (1971). *Acta Cryst.* **B27**, 1864–1867.

GLAZER, A. M. (1972). *Acta Cryst.* **B28**, 3384–3392.

International Tables for X-ray Crystallography (1974). Vol. IV. Birmingham: Kynoch Press.

IYER, P. N. & SMITH, A. J. (1967). *Acta Cryst.* **23**, 740–746.

JONA, F., SHIRANE, G., MAZZI, F. & PEPINSKY, R. (1957). *Phys. Rev.* **105**, 849–856.

KATZ, L. & MEGAW, H. D. (1967). *Acta Cryst.* **22**, 639–648.

KOVBA, L. M. & TRUNOV, V. K. (1962). *Dokl. Akad. Nauk SSSR*, **147**, 622–624.

LABEAU, M. (1980). PhD thesis, Univ. Grenoble.

LABEAU, M., GREY, I. E., JOUBERT, J. C., VINCENT, H. & ALARIO-FRANCO, M. A. (1982). *Acta Cryst.* **A38**, 753–761.

ROSSELL, H. J. & SCOTT, H. G. (1975). *J. Solid State Chem.* **13**, 345–350.

SAKOWSKI-COWLEY, A. C., LUKASZEWICZ, K. & MEGAW, H. D. (1969). *Acta Cryst.* **B25**, 851–865.

STEWART, J. M. (1976). Editor. The *XRAY* system - version of 1976. Tech. Rep. TR-446. Computer Science Center, Univ. of Maryland, College Park, Maryland.

TRUNOV, V. K. & KOVBA, L. M. (1966). *Zh. Strukt. Khim.* **7**, 896–897.

ZACHARIASEN, W. H. (1978). *J. Less-Common Met.* **62**, 1–7.